

ULTRASOUND-ASSISTED CONVENTIONAL SINTERING OF SILICATE CERAMICS

#SHU LIAO, HENG ZHANG, BI JIA, HUIMING WU, #YONGJIANG DI, #XIN WAN, BIAO LIU

Chongqing Key Laboratory of Nano-Micro Composite Materials and Devices, School of Metallurgy and Materials Engineering, Chongqing University of Science and Technology, Chongqing 401331, China

#E-mail: yjdee@163.com; wanxin288@163.com

Submitted October 12, 2022; accepted November 16, 2022

Keywords: Ultrasonic vibration, Activation sintering, Silicate ceramics

An ultrasonic-assisted resistance sintering furnace was developed by using an integrated crucible to transfer ultrasonic energy to silicate ceramic samples for improving the conventional sintering process. The silicate ceramic samples were prepared and sintered by conventional and ultrasound-assisted sintering processes. The shrinkage, water absorption, bulk density, crystalline phase, and morphology were investigated by using the Archimedes method, X-ray diffraction, and scanning electron microscopy. The results show that the densification and microstructure of the samples can be improved by the ultrasound-assisted sintering at lower sintering temperatures and sintering times. The optimum sintering temperatures in this study were 1160 °C and 1145 °C for the conventional and ultrasound-assisted sintering processes, respectively. The loading of ultrasonic waves in the sintering can homogenise the grain size and grain shape, and make the grain and pore distribution more uniform. The microstructure is remarkably improved at the appropriate sintering temperature and sintering times by ultrasonic-assisted sintering.

INTRODUCTION

Ceramics are essential materials with a wide range of applications due to their high mechanical, thermal, and chemical stability [1–2]. The sintering process plays a crucial role in the preparation of ceramics. However, the microstructure of ceramics is limited by the sintering methods used in conventional sintering (CS) techniques. Researchers have developed many new sintering techniques, such as microwave-assisted sintering [3–4], spark plasma sintering (SPS) [5–6], flash sintering [7–10], ultrafast high-temperature sintering [11], and other sintering methods [12–13] through extensive efforts. The microwave-assisted sintering and SPS techniques require expensive commercial equipment. The recently developed flash sintering and rapid thermal annealing

methods have shown high heating rates suitable for many ceramics, but need complex equipment [11]. Ultrasonic techniques have widely been used for molten alloy material preparation and heat treatment [14–19]. However, ultrasonic-assisted sintering techniques are only available at a few hundred degrees Celsius in the current studies [20–23].

To overcome the limitations of conventional sintering, we developed an ultrasound-assisted sintering technique that can be used to assist conventional ceramic sintering by the activation of ultrasonic vibration. We set up an ultrasound-assisted sintering furnace to sinter ceramics. In this work, the ultrasound-assisted CS (UCS) of silicate ceramics was compared with CS to understand the effect of ultrasonic vibrations on the CS process.

EXPERIMENTAL

Constituents

The silicate ceramics with a formula of 44 % kaolin, 37 % quartz, 16 % potassium feldspar, and 3 % bentonite were prepared by ball milling, sieving, and drying the raw materials. Press forming was used with a forming pressure of 3 MPa and a dwell time of 20 s. The samples were sintered by UCS and CS techniques in an air atmosphere with temperatures from 1050 °C to 1250 °C with a heating and cooling rate of 5 °C·min⁻¹ with three dwell times (5, 15, and 30 min). The schematics of the UCS furnace are shown in Figure 1.

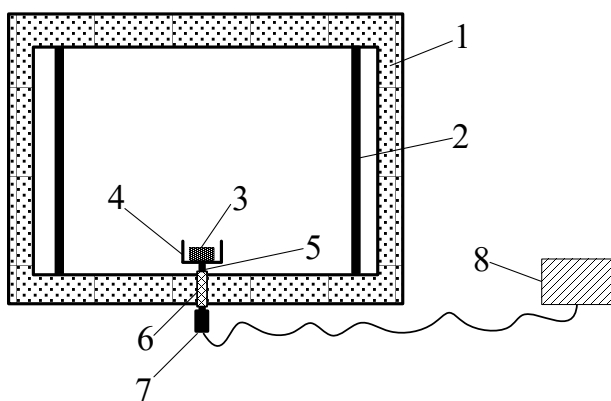


Figure 1. Schematics of the UCS furnace (1-sintering house, 2-heating body, 3-pellet sample, 4-diaphragm, 5-ultrasonic conducting rod, 6-conducting rod supporting frame, 7-ultrasonic transducer, 8-ultrasonic generator)

The ceramic pellet samples were placed in the diaphragm of the UCS furnace. The ultrasonic wave was conducted to specimens, and the ultrasonic generator was started during the dwelling procedure to assist the sintering during the UCS process. CS was applied at the same condition without ultrasonic wave assisting.

The dimensional changes to the specimens were measured before and after sintering, and the linear shrinkage was calculated. The water absorption and bulk density were measured by using Archimedes' method in water. The crystalline phases were identified by using X-ray diffraction (XRD) with Cu K radiation (SmartLab-9 X-ray) on the bulk samples. The cross-sectional fracture morphology of the samples was characterised by scanning electron microscopy (SEM, JSM-7800F).

RESULTS AND DISCUSSION

Crystal phase development with temperature

The crystal phase of the samples sintered at different temperatures by UCS and CS is shown in Figure 2. The relative intensity of the SiO₂ and Na₆Si₈O₁₉ crystal phase diffraction peak in the ceramics was chosen to analyse the crystal phase development with the temperature.

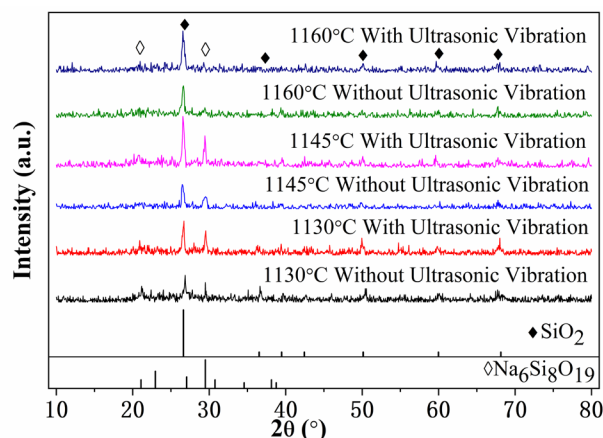


Figure 2. XRD pattern of the sintered samples at the different temperatures.

As shown in Figure 2, the relative SiO₂ intensity increases with an increase in the temperature for the UCS and CS. By contrast, the relative Na₆Si₈O₁₉ intensity first increases and then disappears with an increase in the temperature for the UCS and CS. The disappearance of Na₆Si₈O₁₉ at 1160 °C may be the transformation of the crystal phase to the glass phase, which can be observed from the SEM image. The intensity peaks of SiO₂ and Na₆Si₈O₁₉ are higher for the UCS, which indicates that the UCS promotes the crystallisation of the silicate ceramics at an optimal sintering temperature. The effect of the ultrasonic activation on the sintering weakens with the increase in the temperature.

Morphology development with temperature

In the SEM image of the CS samples in Figures 3, 4, and 5, the UCS sample has more and larger crystalline grains at 1130 °C than the CS sample. The UCS sample has fewer large pores and an optimal grain arrangement at 1145 °C than the CS sample. With the increase in temperature to 1160 °C, the glass phase in the sample gradually increased, and the tightness of the arrangement of the grains steadily decreased in the UCS and CS. The UCS has more glass phases than the CS in all the sintering cases.

As shown in the SEM image in Figures 3, 4, and 5, the UCS sample at 1145 °C has the best grain size and tighter arrangement. This finding shows that the densification of the UCS sample at this temperature is the best, which is consistent with the data of the UCS sample at 1145 °C in Figure 5.

As shown in Figure 3, the pores of the sample after the UCS are significantly larger than those of the CS sample when the sintering temperature is 1130 °C. The grain size is small, and combining the crystal grains with the CS sample, it is superior to the samples sintered with the UCS. This finding is consistent with the analysis of the bonding and grain growth between the UCS disrupted

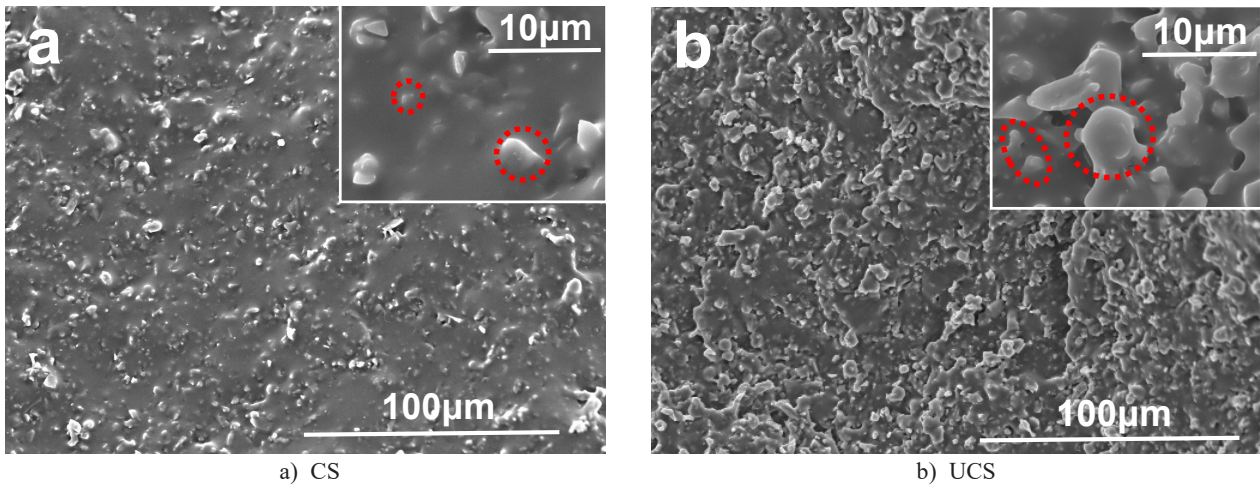


Figure 3. SEM image of the sintered sample at 1130 °C for 60 min with the CS (a) and UCS (b).

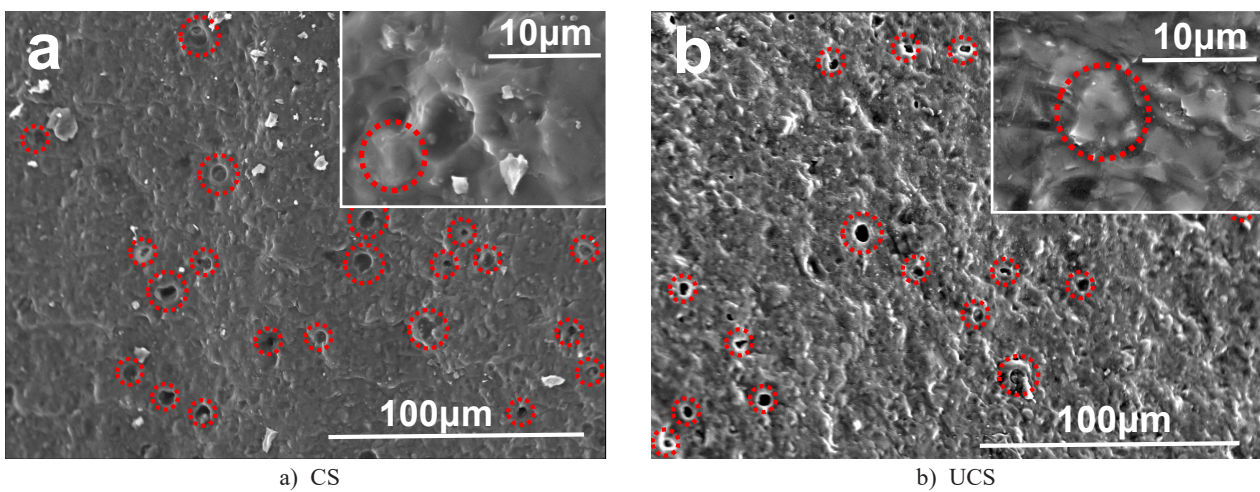


Figure 4. SEM image of the sintered sample at 1145 °C for 60 min with the CS (a) and UCS (b)

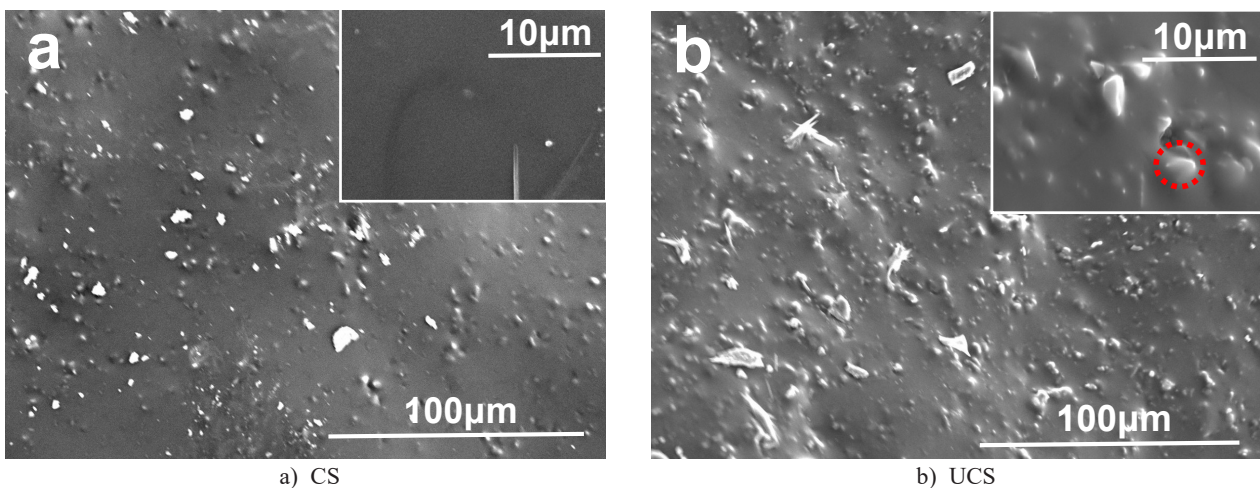


Figure 5. SEM image of the sintered sample at 1160 °C for 60 min with the CS (a) and UCS (b).

particles when the sintering temperature in Figure 6 is lower than 1130 °C.

The UCS sample shows fewer pores than the CS sample, and the grain size is larger than that of the CS sample at the two temperatures of 1145 °C and 1160 °C. The liquid-phase quantity increases in the sample

when the temperature rises. The cavitation effect of the ultrasonic wave then forces the liquid phase to fill the pores in the sample. The driving force of the grain boundary movement is consistent with the favourable analysis results of the grain growth.

Densification characteristics with temperature

The shrinkage, water absorption, and bulk density of the specimens sintered with the UCS and CS methods at temperatures of 1100 °C, 1115 °C, 1130 °C, 1137 °C, 1145 °C, 1152 °C, and 1160 °C were investigated, as shown in Figure 6.

The shrinkage and bulk density increase, whereas the water absorption decreases with the increase in the temperature for the UCS and CS. In the case of the UCS, the samples sintered at 1145 °C have the highest density and lowest water absorption, indicating that the grain growth of the sample is at its highest in good condition, and the elimination of stomata is considerable. However, the shrinkage and density of the sample remarkably decrease after exceeding 1145 °C. In the case of the CS sample, the highest porosity appears at 1160 °C. This condition may be due to an excessively high sintering temperature, resulting in an increase in the number of glassy phases in the sample (liquid-phase at high temperature) and a slight increase in the pores, which may be caused by the excessively high temperature at 1160 °C. The phase increased to a certain extent, and the viscosity became small. Therefore, the flow mass-energy increased, and the elimination of stomata was promoted. The density of the pure glass phase is lower than that of the crystal phase. Thus, the increase in the glass phase leads to a decrease in the shrinkage rate. Therefore, 1145 °C is the optimum sintering temperature for the CS.

Ultrasound-assisted sintering suppresses the densification process of the silicate ceramic samples before reaching 1130 °C, which may be because the ultrasound disrupts the bond between the grains and the growth of the grains during the vibration process. The UCS at higher sintering temperatures of 1130 °C, 1145 °C, and 1160 °C resulted in increased liquid phase. The liquid phase in the sample filled the pores in the sample sufficiently, and the liquid phase increased because of the cavitation effect of the ultrasonic waves. This condition also increased the driving force of the grain boundary diffusion, which made the densification of the UCS silicate ceramic samples take shorter than the CS silicate ceramic samples. The densification effect of the UCS at 1145 °C is the most obvious. The sample's

shrinkage, density, and water absorption are the best among the UCS temperature and the CS temperature. When the temperature exceeds 1145 °C, the liquid phase in the sample becomes excessive, and the viscosity becomes smaller, which causes the sample to expand and deform. This condition affects the densification of the sample, resulting in a decrease in the densification. As shown in Figure 6, the shrinkage and density of the sample at the sintering temperature of 1145 °C began to decrease, and the water absorption began to increase.

Crystal phase development with dwell time

The XRD pattern of the sintered sample for the different dwell times is shown in Figure 7. When the UCS is performed for 30, 60, and 120 min, the types and contents of the crystal phases generated in the silicate ceramic are the same. They all show SiO₂ and Na₆Si₈O₁₉ for several materials, and the effect of the dwell time for 10 and 20 min had a minimal effect on the crystallisation of the silicate ceramics.

As shown in Figure 7, the intensity of the crystal phase diffraction peak of the sample after the UCS is higher than that of the CS sample from 30 min of incubation to 60 min of incubation. In particular, the intensity of the diffraction peak is much higher between 30 and 60 min of incubation, and the difference is

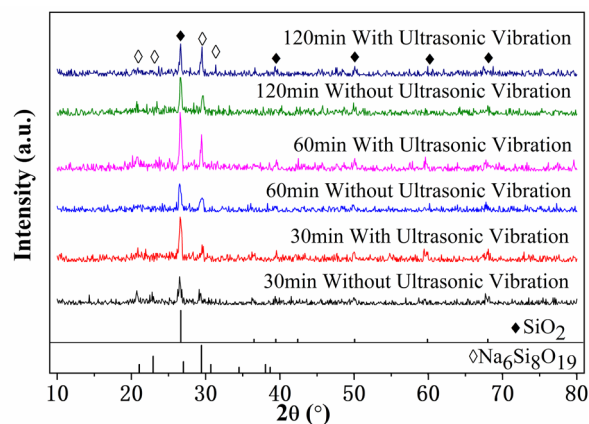


Figure 7. XRD pattern of the sintered samples at the different dwell times.

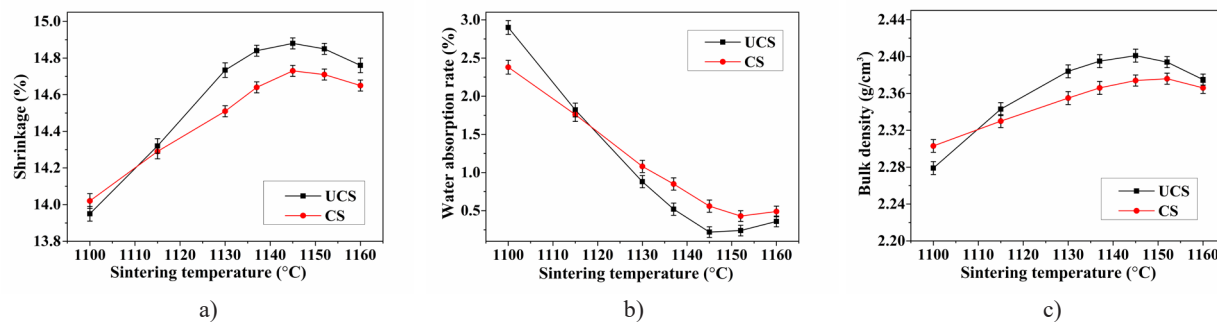


Figure 6. Shrinkage, water absorption, and bulk density of the sintered samples at the different temperatures.

insignificant at 90 min of incubation. When the dwell time is increased to 120 min, the intensity of the diffraction peak of the UCS is higher than that of the CS.

As shown in Figure 7, the $\text{Na}_6\text{Si}_8\text{O}_{19}$ crystal phase content in the UCS sample increases first and then decreases with the increase in the dwell time. The highest content of the $\text{Na}_6\text{Si}_8\text{O}_{19}$ crystal phase in the three dwell times is 60 min, so the best dwell time is the content of the $\text{Na}_6\text{Si}_8\text{O}_{19}$ crystal phase, which is higher than that of the CS at 1145 °C for 60 min.

Morphology development with dwell time

The SEM images of the CS and UCS samples at the different dwell times are shown in Figures 8, 9, 10, and 11.

In the SEM image with a magnification of 500×, no pores are observed when the UCS sample is incubated for 30 min in comparing Figures 9 to 11. The pores in the CS sample are huge, indicating that the UCS is extremely advantageous for the densification of the ceramics. However, the pores of the two SEM specimens

are noticeable when the dwell time was 120 min, indicating that the gas phase is concentrated. The UCS pores are more common than the CS pores, but the pore size is uniform, indicating that the UCS has a remarkable liquid-phase content.

The glass phase in the silicate ceramics gradually decreases, the grain distribution is more uniform, and the arrangement is tighter and more regular with the increase in the dwell time before the UCS for 60 min. As the content of the glass phase in the dwelling procedure for 120 minutes increases, the grains become smaller, and the crystal grains are not prominent.

Densification characteristic with dwell time

For the sintering temperature of 1145 °C, the test results of the water absorption and bulk density of the CS and UCS silicate ceramic samples with the different dwell times are shown in Figure 12.

The shrinkage rate and bulk density increase with the increase in the dwell time, and the UCS load

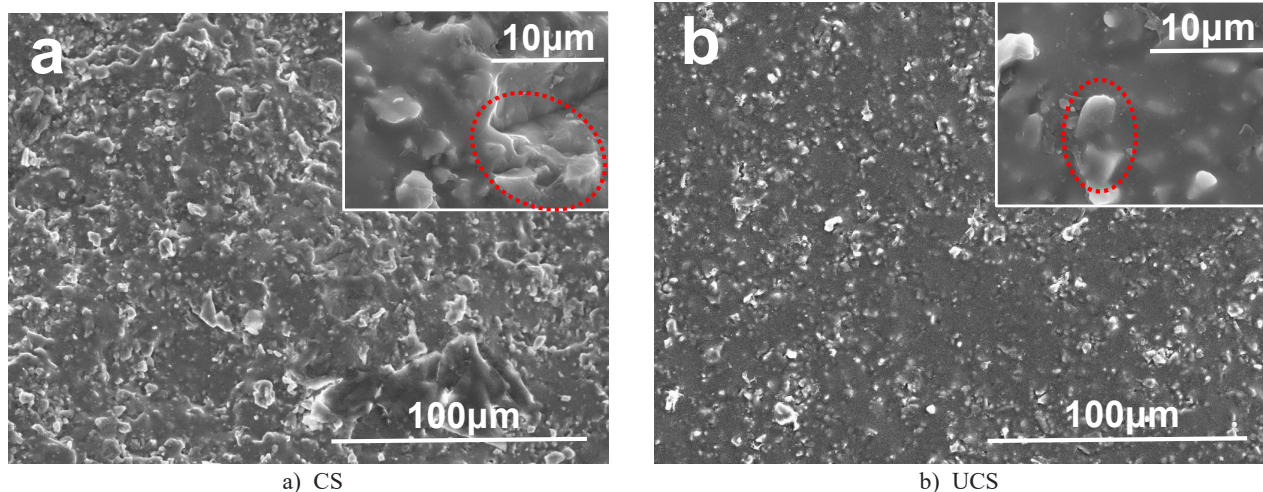


Figure 8. SEM image of the sintered sample at 1145 °C for 10 min with the CS (a) and UCS (b).

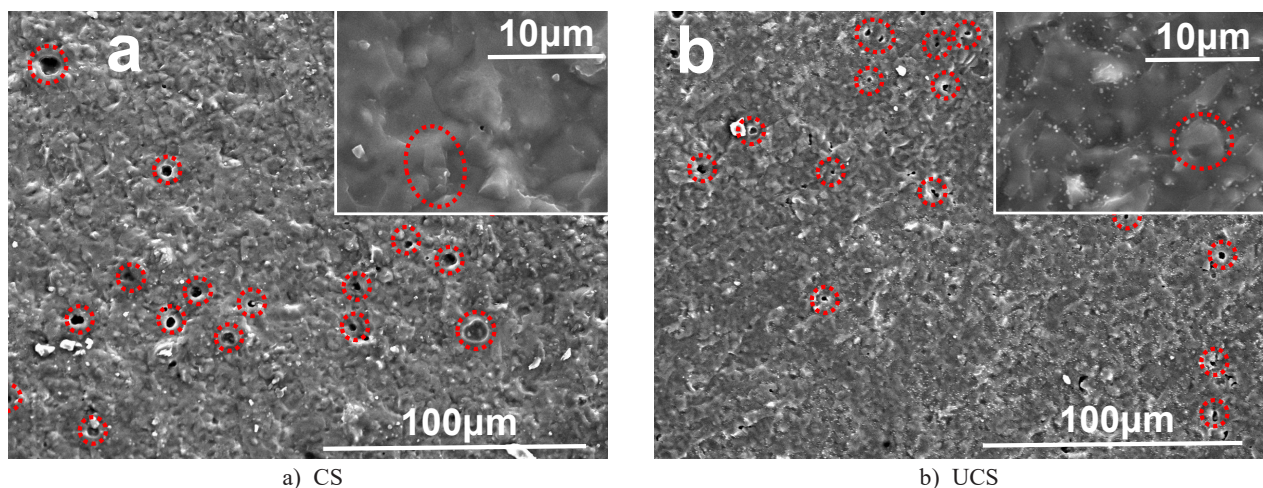


Figure 9. SEM image of the sintered sample at 1145 °C for 30 min with the CS (a) and UCS (b).

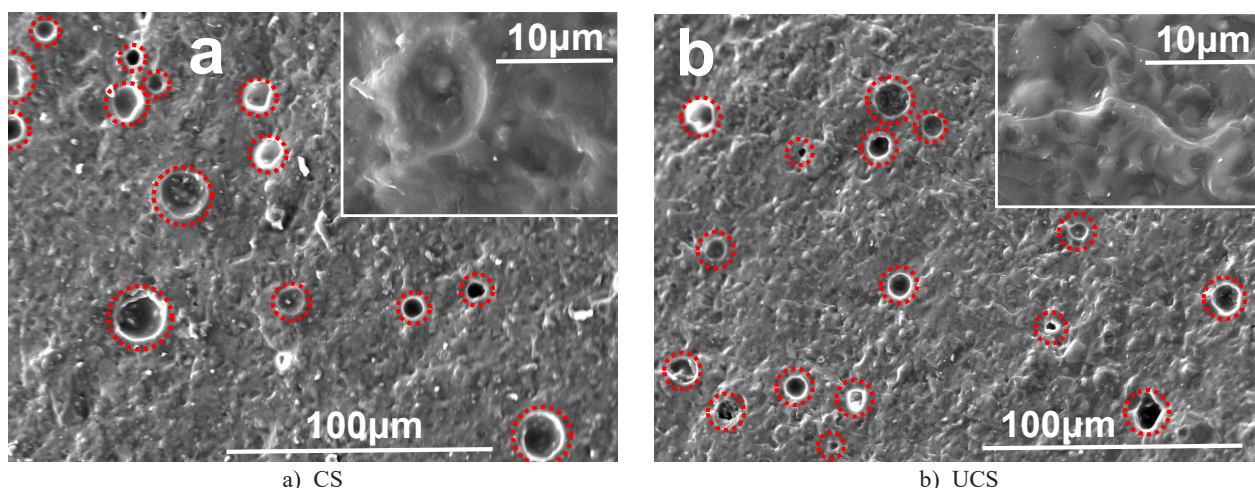


Figure 10. SEM image of the sintered sample at 1145 °C for 60 min with the CS (a) and UCS (b).

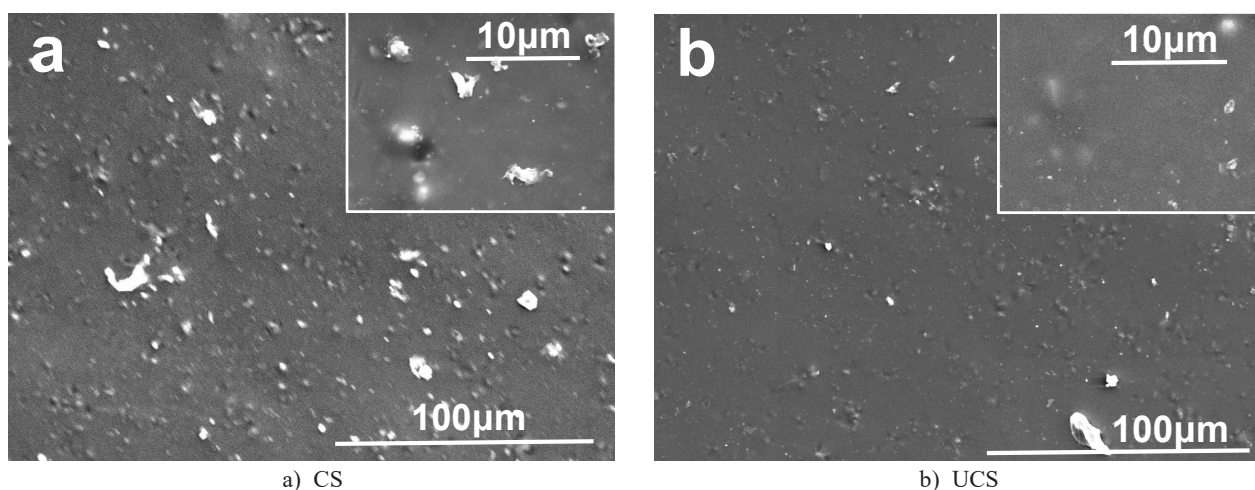


Figure 11. SEM image of the sintered sample at 1145 °C for 120 min with the CS (a) and UCS (b).

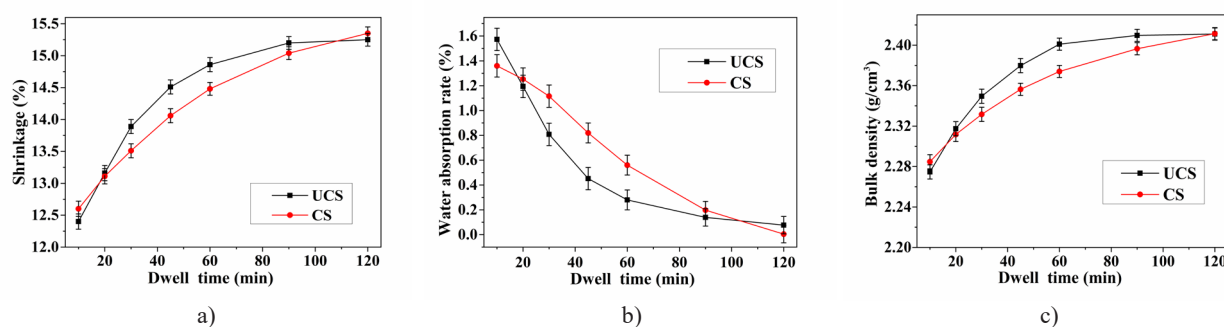


Figure 12. Shrinkage, water absorption, and bulk density of the sintered samples at the different dwell times.

before 45 min is more remarkable than that of the CS sample. The ceramic sample loaded with the ultrasonic wave shrinks after 45 min. The rate is lower than that of the CS sample. The bulk density variation rule is the same, except that the dwell time is 60 min. This finding shows that increasing the dwell time is beneficial to the densification of the silicate ceramics.

Therefore, the UCS is beneficial to densifying silicate ceramics before dwelling for 90 min. The UCS is uncondusive to the densification of silicate ceramics after dwelling for 90 min.

Kinetics of UCS and CS

The effects of the dwell time on the shrinkage rate of the UCS and CS samples at 1145 °C were substituted into the sintering kinetic equation [24]

$$\lg(\Delta L/L_0) = n \lg t + \lg k \quad (1)$$

where $\Delta L/L_0$ is the shrinkage rate, n is the sintering kinetic characteristic index, t is the dwell time, and k is the equilibrium constant.

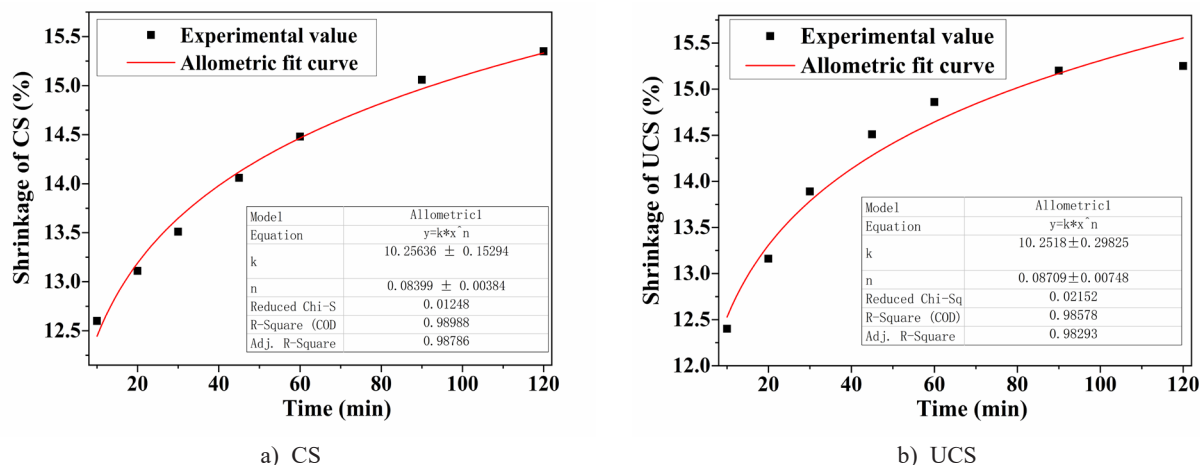


Figure 13. Schematic of the kinetics of the CS (left) and UCS (right).

The data were loaded into Equation 1 to perform the fitting process, as shown in Figure 13.

As shown in Figure 13, n -ultrasound = 0.08709, k -ultrasound = 10.2518, n -normal = 0.08399, and k -normal = 10.25636.

The values of n and k are substituted into the sintering kinetics formula

$$\Delta L/L_0 = A(T)t^{1/n} \quad (2)$$

$$k = \exp(A - Q/RT) \quad (3)$$

where A is a constant, R is a gas constant ($R = 8.314$), T is the sintering temperature (1418 K), and Q is the sintering activation energy (J).

We can calculate $QUCS = 1 \times 10^5$ J and $QCS = 1.2 \times 10^5$ J. The activation energy of the UCS and CS is compared, and the UCS can reduce the activation sintering energy. This finding shows that the UCS is easier to sinter at this temperature.

In accordance with the sintering kinetics, the sintering is assumed to be dominated by volume diffusion, which is close to Kings' kinetic equation. Combined with the SEM and XRD patterns, the liquid phase has more crystal phases, and the high-frequency ultrasonic vibration is favourable to the crystal. The uniform grain growth, low temperature, and short sintering time during the short dwell time indicate that the silicate ceramic sintering of this project is a liquid-phase mass transfer process with a certain liquid-phase content.

For the sample at the sintering temperature, ultrasonic loading can make the sample to be in high-frequency vibration during the high-temperature sintering stage. The action of resistance of the high-temperature thermal radiation and ultrasonic vibration energy coupling helps promote the sintering and densification of the sample. The particles grow rapidly and evenly, the particle size is uniform and refined, and the performance of sintered samples is improved.

CONCLUSION

An ultrasound-assisted sintering techniques has been developed to assist conventional ceramic sintering by the activation of ultrasonic vibration. The assistance of ultrasonic waves can optimise the grain shape, distribution, and pore distribution, resulting in a uniform distribution of the grains and pore sizes and a remarkable improvement in the microstructure at a proper sintering temperature and dwell time. Activation by loading by ultrasound at the appropriate temperature can promote the crystallisation and densification of the sintered samples of silicate ceramics. The most obvious sintering condition for the ultrasonic activation to promote the sintering of silicate ceramics is 1145 °C for 60 min for this subject. The activation energy of the sintering is reduced by loading with ultrasonic waves, where a specific activation effect is observed on the sintering.

Acknowledgements

This research is funded by the Chongqing Research Program of Basic Research and Frontier Technology (No. cstc2016jcyjA0084) and the Research Foundation of Chongqing University of Science & Technology.

REFERENCES

1. Dhuban S. B., Ramesh S., Tan C. Y., Wong Y. H., Alengaram U. J., Ramesh S., Teng W. D., Tarlochan F., Sutharsini U. (2019): Sintering behaviour and properties of manganese-doped alumina. *Ceramics International*, 45(6), 7049–7054. Doi:10.1016/j.ceramint.2018.12.207
2. Vajdi M., Moghanlou F. S., Sharifianjazi F., Asl M. S., Shokouhimehr M. (2020): A review on the Comsol Multiphysics studies of heat transfer in advanced ceramics. *Journal of Composites and Compounds*, 2(2), 35–43. doi:10.29252/jcc.2.1.5

3. Alem S. A. A., Latifi R., Angizi S., Hassanaghaei F., Aghaahmadi M., Ghasali E., Rajabi M. (2020): Microwave sintering of ceramic reinforced metal matrix composites and their properties: a review. *Materials and Manufacturing Processes*, 35(3), 303–327. doi:10.1080/10426914.2020.1718698
4. Curto H., Thuault A., Jean F., Violier M., Dupont V., Hornez J. C., Leriche A. (2020): Coupling additive manufacturing and microwave sintering: a fast processing route of alumina ceramics. *Journal of the European Ceramic Society*, 40(7), 2548–2554. doi:10.1016/j.jeurceramsoc.2019.11.009
5. Hu Z. Y., Zhang Z. H., Cheng X. W., Wang F. C., Zhang Y. F., Li S. L. (2020): A review of multi-physical fields induced phenomena and effects in spark plasma sintering: Fundamentals and applications. *Materials & Design*, 191, 108662. doi:10.1016/j.matdes.2020.108662
6. Mogale N. F., Matizamhuka W. R. (2020): Spark plasma sintering of titanium aluminides: a progress review on processing, structure-property relations, alloy development and challenges. *Metals*, 10(8), 1080. doi:10.3390/met10081080
7. Biesuz M., Sglavo V. M. (2019): Flash sintering of ceramics. *Journal of the European Ceramic Society*, 39(2-3), 115–143. doi:10.1016/j.jeurceramsoc.2018.08.048
8. Biesuz M., Sglavo V. M. (2020): Beyond flash sintering: How the flash event could change ceramics and glass processing. *Scripta Materialia*, 187, 49–56. doi:10.1016/j.scriptamat.2020.05.065
9. Ojaimi C. L., Ferreira J. A., Chinelatto A. L., Chinelatto A. S. A., Pallone E. M. D. J. A. (2020): Microstructural analysis of ZrO₂/Al₂O₃ composite: Flash and conventional sintering. *Ceramics International*, 46(2), 2473–2480. doi:10.1016/j.ceramint.2019.09.241
10. Ren K., Liu J., Wang Y. (2020): Flash sintering of yttria-stabilized zirconia: Fundamental understanding and applications. *Scripta Materialia*, 187, 371–378. doi:10.1016/j.scriptamat.2020.06.040
11. Wang C., Ping W., Bai Q., Cui H., Hensleigh R., Wang R., et al. (2020). A general method to synthesize and sinter bulk ceramics in seconds. *Science*, 368(6490), 521–526. doi:10.1126/science.aaz7681
12. Lóh N. J., Simão, L., Faller, C. A., De Noni Jr, A., and Montedo, O. R. K. (2016). A review of two-step sintering for ceramics. *Ceramics International*, 42(11), 12556–12572. doi:10.1016/j.ceramint.2016.05.065
13. Ndayishimiye A., Sengul M. Y., Bang S. H., Tsuji K., Takashima K., de Beauvoir T. H., Denux D., Thibaud J. M., van Duin A. C. T., Elissalde C., Goglio G., Randall C. A. (2020). Comparing hydrothermal sintering and cold sintering process: Mechanisms, microstructure, kinetics and chemistry. *Journal of the European Ceramic Society*, 40(4), 1312–1324. doi:10.1016/j.jeurceramsoc.2019.11.049
14. Barbosa J., Puga H. (2019): Ultrasonic melt treatment of light alloys. *International Journal of Metalcasting*, 13(1), 180–189. doi:10.1007/s40962-018-0248-x
15. Todaro C. J., Easton M. A., Qiu D., Wang G., StJohn D. H., Qian M. (2019): Effect of ultrasonic melt treatment on intermetallic phase formation in a manganese-modified Al-17Si-2Fe alloy. *Journal of Materials Processing Technology*, 271, 346–356. doi:10.1016/j.jmatprotec.2019.04.008
16. Fong J. F. Y., Chin S. F., Ng S. M. (2015): Facile synthesis of carbon nanoparticles from sodium alginate via ultrasonic-assisted nano-precipitation and thermal acid dehydration for ferric ion sensing. *Sensors and Actuators B: Chemical*, 209, 997–1004. doi:10.1016/j.snb.2014.12.038
17. Marquez-Garcia L., Li W., Bompfrey J. J., Jarvis D. J., Min G. (2015): Preparation of nanoparticles of thermoelectric materials by ultrasonic milling. *Journal of Electronic Materials*, 44(6), 2172–2176. doi:10.1007/s11664-015-3749-x
18. Chen D., Li L., Wang J.H. (2013): One-step synthesis of zinc ferrite nanoparticles by ultrasonic wave-assisted ball milling technology. *Ceramics International*, 39(4), 4669–4672. doi:10.1016/j.ceramint.2012.10.247
19. Chen P., Liao W. B., Liu L. H., Luo F., Wu X. Y., Li P. J., Yang C., Yan M., Liu Y., Zhang L. C., Liu Z. Y. (2018): Ultrafast consolidation of bulk nanocrystalline titanium alloy through ultrasonic vibration. *Scientific Reports*, 8(1), 1–9. doi:10.1038/s41598-018-19190-8
20. Singh G., Pandey P. M. (2020): Neck growth kinetics during ultrasonic-assisted sintering of copper powder. *Proceedings of the Institution of Mechanical Engineers, Part C: Journal of Mechanical Engineering Science*, 234(11), 2178–2188. doi:10.1177/0954406220904108
21. Singh G., Pandey P. M. (2019): Ultrasonic assisted pressureless sintering for rapid manufacturing of complex copper components. *Materials Letters*, 236, 276–280. doi:10.1016/j.matlet.2018.10.123
22. Wang F., Nie N., He H., Tang Z., Chen Z., Zhu W. (2017): Ultrasonic-assisted sintering of silver nanoparticles for flexible electronics. *The Journal of Physical Chemistry C*, 121(51), 28515–28519. doi:10.1021/acs.jpcc.7b09581
23. Liu Z., Ge Y., Zhao D., Lou Y., Liu Y., Wu Y., Yu P., Yu C. (2020): Ultrasonic assisted sintering using heat converted from mechanical energy. *Metals*, 10(7), 971. doi:10.3390/met10070971
24. Liu C., Sun J., Xie Z. (2013): Microstructures and sintering kinetics of pressureless sintered alumina doped with diopside and AlTiB. *Journal of Alloys and Compounds*, 546, 102–106. doi: 10.1016/j.jallcom.2012.08.097